Study on the Performance of MnFe$_2$O$_4$ as Anode Material for Lithium-Ion Batteries Using Spent Alkaline Zn-Mn Batteries as Manganese Source

Feng Xiao, Guanghui Guo[*], Kang Lu, Jianghua Qiu

Key Laboratory of Hubei Province for Coal Conversion and New Carbon Materials, Wuhan University of Science and Technology, Wuhan 430081, China)
[*]E-mall: guoguanghui@wust.edu.cn

In this work, we report the electrochemical properties of MnFe$_2$O$_4$ as anode materials for lithium-ion batteries using spent Zn-Mn batteries as raw materials by three different methods: sol-gel method, hydrothermal method in glycol and hydrothermal method in water. The materials were characterized by X-ray diffraction (XRD), scanning electron microscopy (SEM), particle size analysis and charge-discharge test. The result showed that the material synthesized by hydrothermal in water shows the best cycle performance of all, the initial discharge specific capacity of MnFe$_2$O$_4$ prepared by this process was 1096 mA h g^{-1}. Moreover, even after 100 cycles, the MnFe$_2$O$_4$ electrode remains 150 mA h g^{-1}. These results of this investigation demonstrate that the process MnFe$_2$O$_4$ prepared by using the spent Zn-Mn batteries as manganese source presents an alternative way for spent alkaline Zn-Mn batteries recycling.

Keywords: Zinc-manganese battery, MnFe$_2$O$_4$, lithium–ion batteries.

1. INTRODUCTION

With the increasing demand of world energy consumption, rechargeable lithium-ion batteries have led the further research efforts on the development of electrode materials with high storage capacity and cycling stability [1-3]. Among numerous candidates of anode materials, transition metal oxides are considered to be promising substitutions for commercial graphite because of their high theoretical capacity [4,5]. As one of the binary metal oxides, MnFe$_2$O$_4$ has been familiar with us mainly because of its attractive magnetic and electromagnetic properties, which made a promising candidate for application in microwave devices and magnetic storage instruments [6,7]. Recently, it

has been proposed as a promising anode for Li-ion batteries due to its low intercalation potential for lithium ions, high theoretical capacity of 926 mA h g^{-1}, environmental benignity and low cost [8-10].

In recent years, as a common primary energy Zn-Mn battery is widely used in portable electronic various products because of the low maintenance, reduced cost and its requirements by the electronics industry [11,12]. However, many spent batteries like alkaline batteries are landfilled or incinerated, instead of being recycled timely. The metals of spent batteries can pose significant environmental and health threats due to their toxicity, abundance and permanence [13]. The removal and recovery of valuable and toxic metals such as Zn, Mn, Li, Co, Ni and Cd from spent batteries including Zn-Mn batteries, Ni-Cd batteries and Li-ion batteries has been a subject of intense interest in the area of solid waste treatment [14]. Many processes for the recycling of batteries have been proposed, but there still have been some imperfections. For example, these approaches often need high recovery processing requirements, and don't produce high value-added products [15,16]. In this paper, MnFe$_2$O$_4$ anode materials for rechargeable lithium ion batteries were prepared by hydrometallurgy recycling technology utilizing spent alkaline Zn-Mn batteries as raw materials.

2. EXPERIMENTAL SECTION

2.1 Battery disposal

Spent alkaline Zn-Mn batteries from several manufactures used as raw materials were manually dismantled, then the washing treatment was carried out to separate plastic films, the ferrous scraps and paper pieces. The mercury removal was carried out by calcining the residues with a tube furnace at 750 °C for 4 h in a constant air flow.

2.2 Recovery of the manganese powder

In this paper, a hydrometallurgical route is proposed to recover manganese from spent alkaline Zn-Mn batteries. The route comprises the steps schematically shown in Fig. 1. The leaching step is conducted in 1:3(v/v) nitric acid under constant magnetic stirring at 60 °C for 5 h, and 3% H$_2$O$_2$ was added in drops during stirring, thus resulted in a solution containing Fe(NO$_3$)$_3$ and Mn(NO$_3$)$_2$ after filtration. The separation of manganese can be achieved by adjusting pH of the filtrate to 6 with NaOH, then the resulting solution was filtered repeatedly. Finally, MnCO$_3$ powder was got after excessive sodium carbonate was added into the filtered solution.

2.3 Synthesis of MnFe$_2$O$_4$

We used three methods to synthesize MnFe$_2$O$_4$: sol-gel method, hydrothermal method in glycol and hydrothermal method in water.

2.3.1 Sol-gel method(SM):

Stoichiometric amount of $MnCO_3$ and $Fe(NO_3)_3 \cdot 9H_2O$ were dissolved in deionized water, and citric acid was added drop-wise, followed by magnetically stirring at 60 °C until the solution was homogeneous, then add 5 ml ethylene glycol and raise the temperature to 90 °C for 3 h. The resultant solution was evaporated at 125 °C for 10 h until a gel was obtained. Then the dried gel was fully ground and calcined in muffle furnace at 500 °C for 4 h. The final product $MnFe_2O_4$ was obtained through air-cooling environment.

2.3.2 Hydrothermal method in glycol(HMG)

Use 1 mol·L^{-1} nitric acid to dissolve the mixture of 0.2 g $MnCO_3$, 1.4 g $Fe(NO_3)_3 \cdot 9H_2O$, 20 ml glycol and 1.5 g CH_3COONa, followed by stirring for half an hour, then transferred the mixed solution into the hydrothermal reactor. After reaction at 180 °C for 10 h, the solid samples were collected and calcined at 500 °C for 1 h.

2.3.3 Hydrothermal method in water(HMW)

First, $MnCO_3$ was firstly dissolved 1 mol·L^{-1} nitric acid, and the as-obtained solution was added 1.4 g $Fe(NO_3)_3 \cdot 9H_2O$ and 10 ml H_2O. During the above mixtures, the molar Mn/Fe (R $_{Mn/Fe}$) ratio was kept 1:2. Then, the suspension was added 2 mol·L^{-1} sodium hydroxide solution drop by drop with constant stirring, and transferred to a 100 mL Teflon-lined stainless-steel autoclave, being kept at 180 °C for 10 h. Next, the products were filtered and calcined at 500 °C for 1 h.
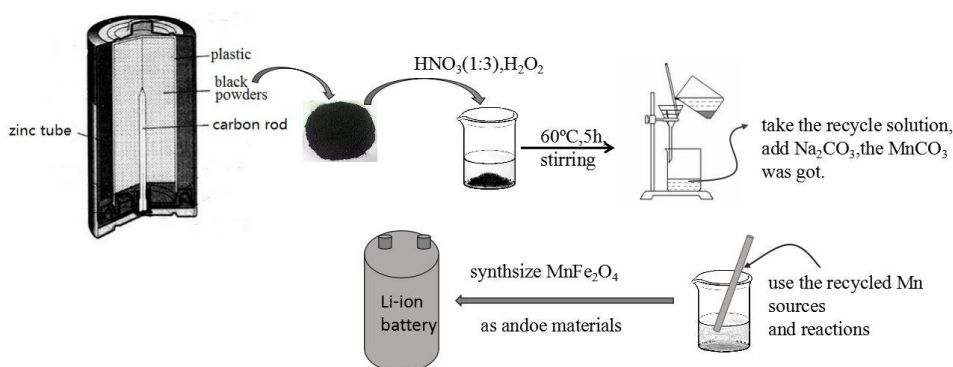

Figure 1. Schematic illustration of the process of recycling spent batteries and synthesizing $MnFe_2O_4$.

2.4 Characterization

X-ray power diffraction was performed using an Xpert-Pro diffractometer with Cu Kα radiation with 2θ values from 10 to 70°. Sample morphology was observed through a scanning electron microscope (SEM, Nova 400 NanoSEM).

2.5 Electrochemical evaluation

The anode was prepared with 75 wt% active materials, 20 wt% acetylene black and 5 wt% polytetrafluoroethylene. The electrochemical measurements were carried out with CR2016 coin cells with lithium wafers as positive pole and 1.0 M $LiPF_6$ as the electrolyte by a LAND CT2001A automatic battery tester system at room temperature, the cycle experiment was conducted between 0.1 and 2.9 V.

3. RESULTS AND DISCUSSION
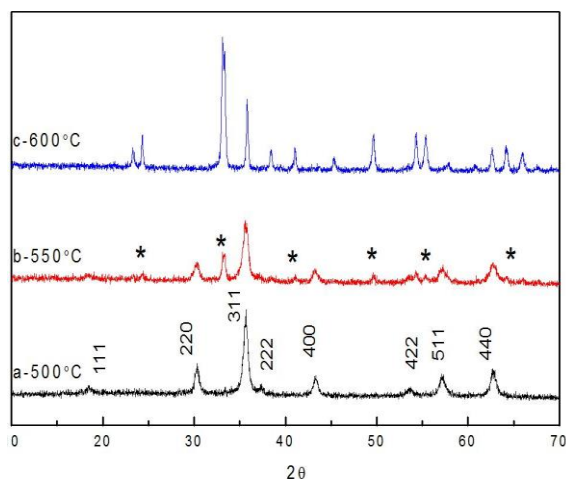
3.1. Structural and morphology characterization

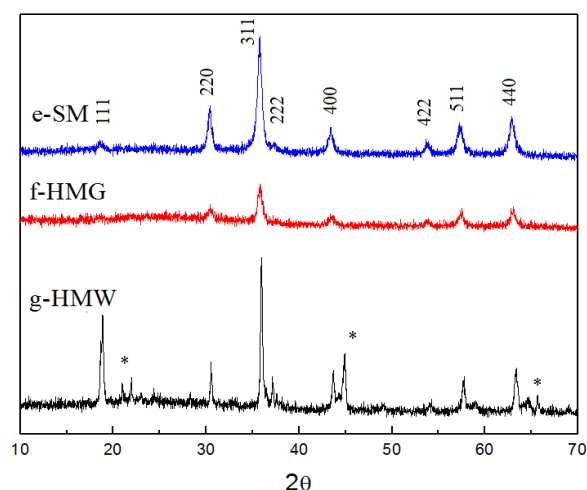**Figure 2.** XRD patterns of the obtained powders calcinated at (a)500 °C, (b)550 °C, (c)600 °C by Sol-gel method

Figure 3. XRD patterns of $MnFe_2O_4$ powders synthesized by (e) SM, (f)HMG, (g)HMW

Fig. 2 is the XRD patterns of the $MnFe_2O_4$ powders synthesized by Sol-gel method (SM) calcinated at (a) 500 °C, (b)550 °C and (c)600 °C. All the diffraction peaks in curve (a) can be indexed to the $MnFe_2O_4$ (JCPDS card No.74-2403). But there is impurity in the powders calcinated at (b)550

°C and (c)600 °C, $MnFe_2O_4$ was oxidized in air when temperature above 550 °C. The peaks marked " ＊ " in curve(b) belong to Fe_2O_3 and Mn_2O_3. The strongest peak of Fe_2O_3 and Mn_2O_3 is at 32.95 °, 33.1 °, respectively, which is just as shown in curve(b), the two peaks coincided around 33 °, and its intensity strengthened with the increase of temperature.

Fig. 3 shows the $MnFe_2O_4$ powders synthesized by (e) SM, (f) HMG and (g) HMW. The curve(e) and (f)'s peaks are indexed to the $MnFe_2O_4$, and no impurity peak can be detected in the samples. By comparison, in curve(g) XRD patterns exhibited Fe_2O_3 peaks near to 20 ° besides $MnFe_2O_4$, because in water system, $Fe(OH)_3$ appeared when NaOH was added, and some of them has formed Fe_2O_3 rather than reacted with Mn^{2+}.
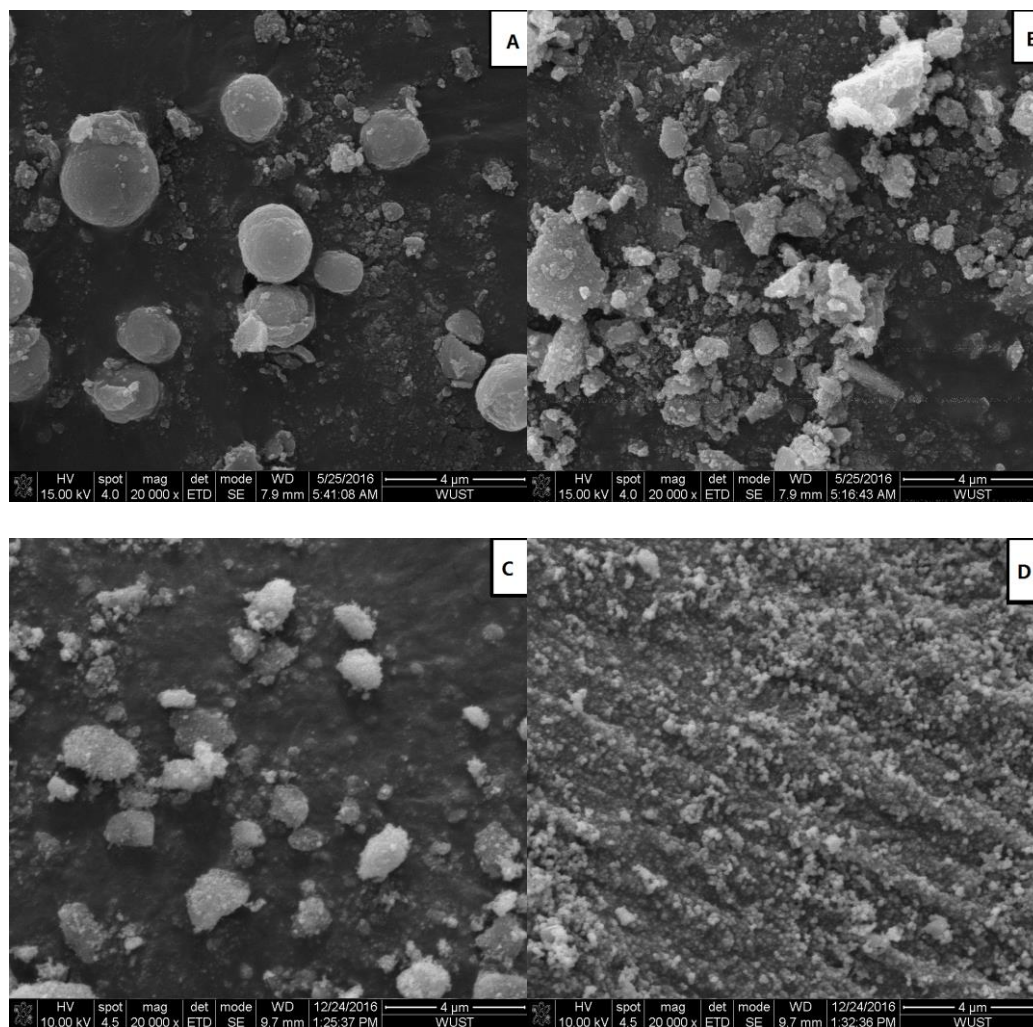

Figure 4. SEM images of obtained $MnCO_3$(A) and $MnFe_2O_4$ synthesized by SM(B), HMG(C), HMW(D).

Fig. 4 displays the SEM images of obtained $MnCO_3$(A) and $MnFe_2O_4$ synthesized by SM(B), HMG(C), HMW(D). The $MnCO_3$ from spent Zn-Mn batteries presents spherical morphology and well distributed particle size of about 2-3 μm. The $MnFe_2O_4$ synthesized by SM(B) and HMG(C) is bad distributed, and shows a low degree of agglomeration.
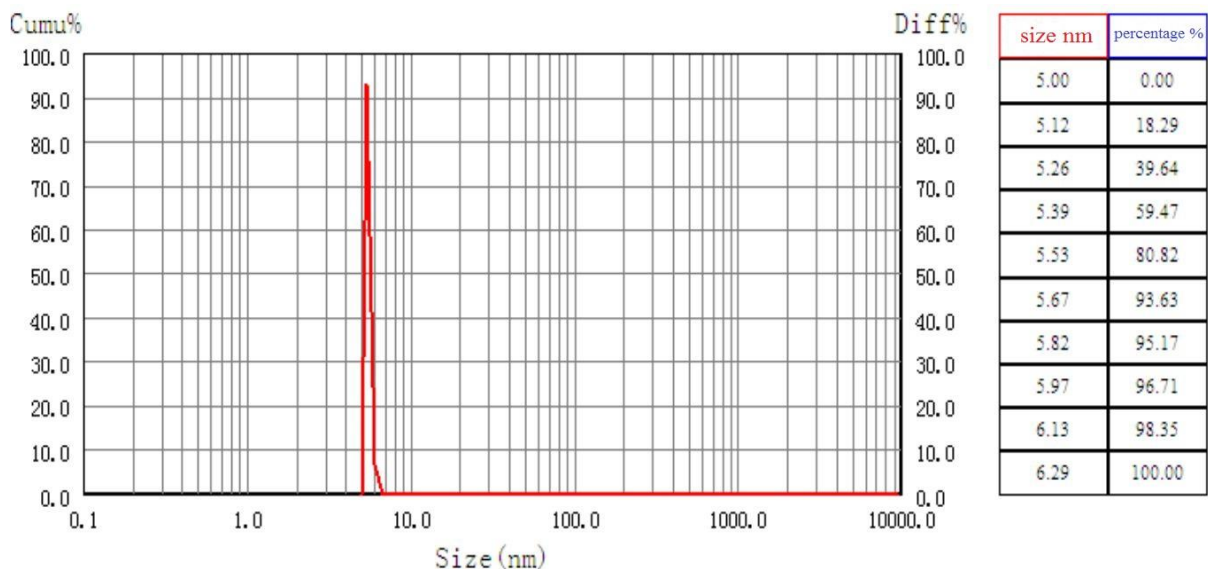
size nm	percentage %
5.00	0.00
5.12	18.29
5.26	39.64
5.39	59.47
5.53	80.82
5.67	93.63
5.82	95.17
5.97	96.71
6.13	98.35
6.29	100.00

Figure 5. The particle size analysis of $MnFe_2O_4$ synthesized by HMW.

Fig. 5 shows the particle size distribution of the powders synthesized by HMW, the average particle size is 5.32 nm, and D90 shows 5.59 nm, the specific surface area of the material is 1024.25 $m^2 \cdot g^{-1}$. This result is similar to the conclusion of Monica Popa [17], the big specific surface area is conducive to the intercalation/deintercalation behavior of Li ion [18].
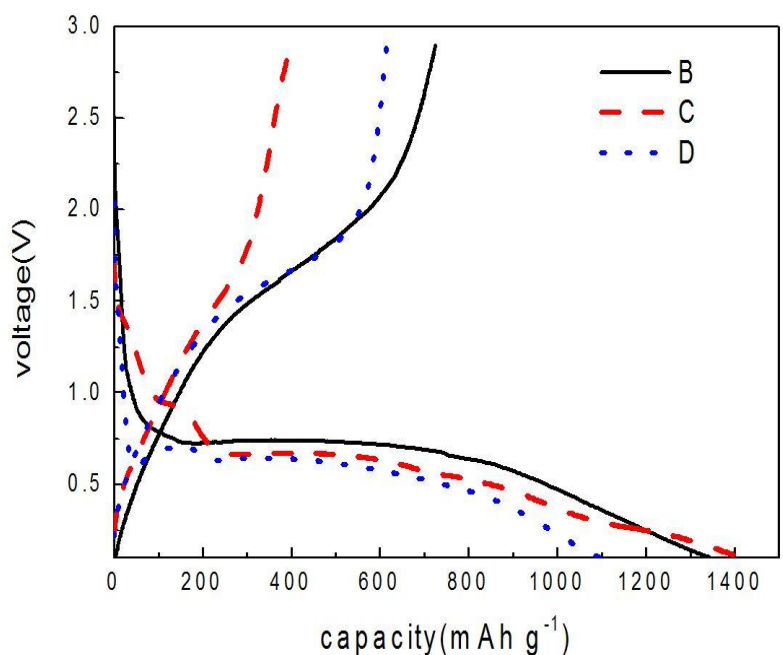
3.2 Electrochemical studies

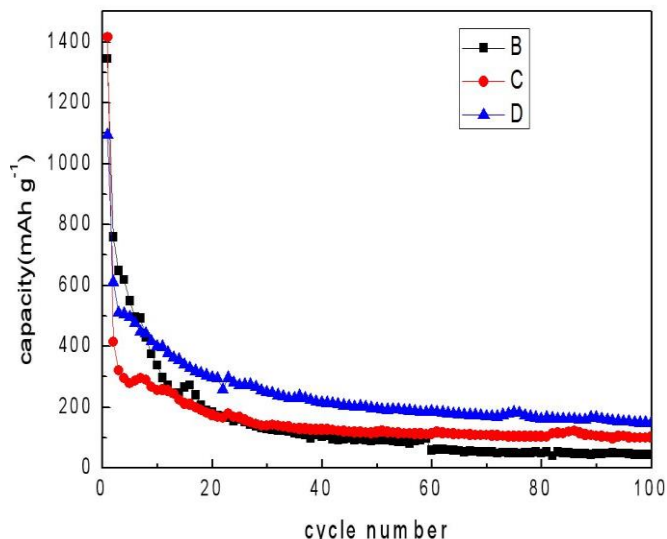**Figure 6.** The initial charge-discharge curves of $MnFe_2O_4$ synthesized by (B)SM, (C)HMG, (D)HMW

Figure 7. The cycling performance of MnFe$_2$O$_4$ synthesized by (B)SM, (C)HMG, (D)HMW at 0.1 A g^{-1}

The practical capacity of synthesized powders was investigated using the Li// MnFe$_2$O$_4$ cells subject to constant current cycling. The Li metal acted as both working and reference electrodes, while MnFe$_2$O$_4$ was treated as the counter electrode. Fig. 6 shows the initial charge-discharge curves of MnFe$_2$O$_4$ synthesized by Sol-gel method(B), hydrothermal method in glycol(C) and hydrothermal method in water(D), with a current density of 100 mA g^{-1} between 0.1 and 2.9 V. It is obvious that all the samples synthesized by three different methods exhibited similar profiles, in the discharge curve all of them have a plateau between the voltage 0.5 and 0.75 V, which represents the typical electrochemical behavior of MnFe$_2$O$_4$ [18,19]. However, different methods represent different electrochemical properties.
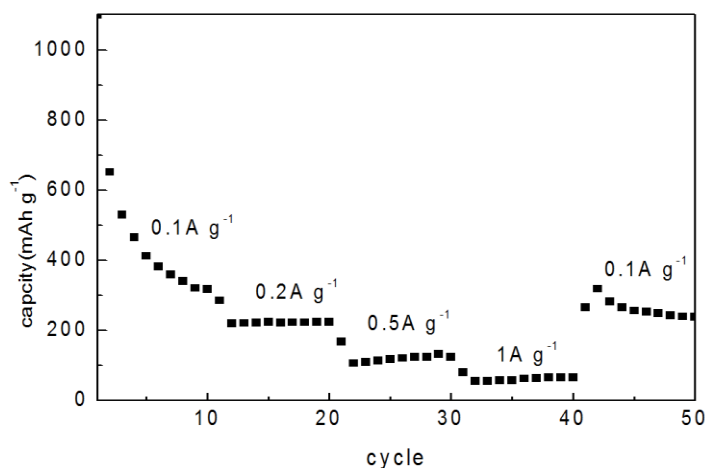

Figure 8. The rate performance of MnFe$_2$O$_4$ synthesized by HMW

The sample synthesized by HMG(C) delivers the largest initial discharge capacity of 1416 mA h g^{-1}, while the samples synthesized by SM(B), HMW(D) show a capacity of 1344 mA h g^{-1}, 1096 mA

h g^{-1}, respectively. The initial charge capacity of SM, HMG, HMW is 712 mA h g^{-1}, 403 mA h g^{-1}, 614 mA h g^{-1}, and the coulombic efficiency of them is 53 %, 28 %, 56 %, respectively. The irreversible capacity loss is mainly attributed to the incomplete conversion reaction and the formation of a solid electrolyte interface (SEI) film during the first cycle [20].

　　　Fig. 7 shows the cyclability of MnFe$_2$O$_4$ synthesized by different method. It is obvious that the powders synthesized by HMW(D) has much better cyclability than the others. After 100 cycles, retentive capacity for SM(B), HMG(C), HMW(D), is about 43 mAh·g^{-1}, 100 mAh·g^{-1},150 mAh·g^{-1}, respectively. It can owe to the particle size of the powders. The MnFe$_2$O$_4$ synthesized by HMW was well distributed and the diameter of it is around 5.5 nm. The MnFe$_2$O$_4$ synthesized by other method presented a low degree of agglomeration, which is harmful to the cyclability of the anode materials. In addition, we made the electrochemical performance comparison between our as-prepared powder synthesized by HMW and other MnFe$_2$O$_4$-based anodes for lithium-ion batteries previously reported, as summarized in Table 1. It is obvious that the powder synthesized by HMW shows about the same reversible capacity compared with others.

Table 1. Electrochemical performance comparison of MnFe$_2$O$_4$-based anodes for lithium-ion batteries

Sample	Raw materials	Synthesis method	Cycle number	Capacity (mA h g^{-1})	Refs.
MnFe$_2$O$_4$	Spent Zn-Mn batteries	HMW	100th	150	This work
MnFe$_2$O$_4$ CNAs	Mn(Ac)$_2$•4H$_2$O	Solvothermal route	100th	~200	[21]
MnFe$_2$O$_4$ cubes	MnSO$_4$	Solvothermal route	50th	~180	[22]
MnFe$_2$O$_4$ nanoparticles	MnSO$_4$	Solvothermal route	60th	~200	[22]

　　　Rate capacity is also an important feature for Li-ion batteries. Fig. 8 shows the rate performance of MnFe$_2$O$_4$ synthesized by HMW at the current density of 0.1 A g^{-1}, 0.2 A g^{-1}, 0.5 A g^{-1}, 1 A g^{-1}. The initial discharge capacity of materials is 1400 mA h g^{-1}, it remains 220 mA h g^{-1} in 10 to 20 cycles at 0.2 A g^{-1}, and even at the high current density of 1 A g^{-1} it remains 65 mA h g^{-1}. And then, it returns to 238 mA h g^{-1} when the current density returns to 0.1 A g^{-1}. The reason of it may attribute to the small size which provide short diffusion length for lithium ions, facilitating the charge/discharge process [23].

4. CONCLUSIONS

　　　The MnCO$_3$ can be easily extracted from the spent Zn-Mn batteries, and it has been used as the manganese source to synthesize MnFe$_2$O$_4$, which provided an alternative way to recycle spent Zn-Mn batteries. Three methods have been implied to synthesize MnFe$_2$O$_4$, the powders synthesized by different method shows different electrochemical properties. Hydrothermal method in water delivers the best cycle performance of all.

References

1. M. Armand, J.M. Tarascon, *Nature,* 451 (2008) 652.
2. Y.G. Guo, J.S. Hu, L.J. Wan, *Adv. Mater.*, 20 (2008) 2878.
3. X. Wu, P. Yan, Y. Yang, Y. Lin, D. Wang, *Ceram. Int.*, 41 (2015) 4080.
4. R. Jin, H. Liu, Y. Guan, J. Zhou, G. Chen, *Mater. Lett.*, 158 (2015) 218.
5. M.M. Rahman, A.M. Glushenkov, T. Ramireddy, T. Tao, Y. Chen, *Naonscale*, 5 (2013) 4910.
6. X. Hou, J. Feng, X. Xu, M. Zhang, *J. Alloys Compd.*, 491 (2010) 258.
7. A.B. Zhang, S.T. Liu, K.K. Yan, Y. Ye, X. G. Chen, *RSC Adv.*, 4 (2014) 13565.
8. N. Wang, X. Ma, Y. Wang, J. Yang, Y. Qian, *J. Mater. Chem*. A, 3 (2015) 9550.
9. S.Y. Liu, J. Xie, Q.M. Su, G.H. Du, S.C. Zhang, G.S. Cao, T.J. Zhu and X.B. Zhao, *Nano Energy*, 8 (2014) 84.
10. K. Zhang, X.P. Han, Z. Hu, X.L. Zhang, Z.L. Tao and J. Chen, *Chem. Soc. Rew*., 44 (2015) 699.
11. E. Sayilgan, T. Kukrer, G. Civelekoglu, F. Ferella, M. Kitis, *Hydrometallurgy*, 97 (2009) 158.
12. J. Wang, Q. Chen, B. Hou and Z. Peng, *Eur. J. Inorg. Chem.*, 45 (2013) 1125.
13. M. Sun, Y. Wang, J. Hong, J. Dai, R. Wang, Z. Niu, B. Xin, *J. Clean. Prod.*, 129 (2016) 350.
14. Z. Niu, Q. Huang, B. Xin, C. Qi, J. Hu, S. Chen, Y. Li, *J Chem Technol Biotechnol.*, 91 (2016) 608.
15. J. Wang, K. Zhang, Z. Peng, Q. Chen, *J. Cryst. Growth*, 266 (2004) 500.
16. S. Chen, G. Guo, F. Liu, *Solid State Ionics*, 261 (2014) 59.
17. M. Popa, P. Bruna, D. Crespo, J. M. Calderon Moreno, *J. Am. Ceram. Soc.*, 91 [8] (2008) 2488.
18. W. Zhang, X. Hou, Z. Lin, L. Yao, X. Wang, Y. Gao& S. Hu, *J Mater Sci: Mater Electron.*, 26 (2015) 9535.
19. Z. Zhang, Y. Wang, Q. Tan, Z. Zhong, F. Su, *J. Colloid Interf Sci.*, 398 (2013) 185.
20. S.Y. Liu, J. Xie, Q.M. Su, G.H. Du, S.C. Zhang, G.S. Cao, *Nano Energy*, 8(2014)84.
21. Y.Q. Cui, F.F. Leng, G.T. Han, G.L. Zhang, H.L. Li, P.Z. Guo, X.S. Zhao, *Int. J. Electrochem. Sci.,* 11(2016)7309.
22. X.M. Lin, X. Lv, L.M. Wang, F.F. Zhang, L.F. Duan, *Mater. Res. Bull.*, 48(2013)2511.
23. Z. Wang, L. Yuan, Q. Shao, F. Huang, Y. Huang, *Mater. Lett.*, 80 (2012) 110.